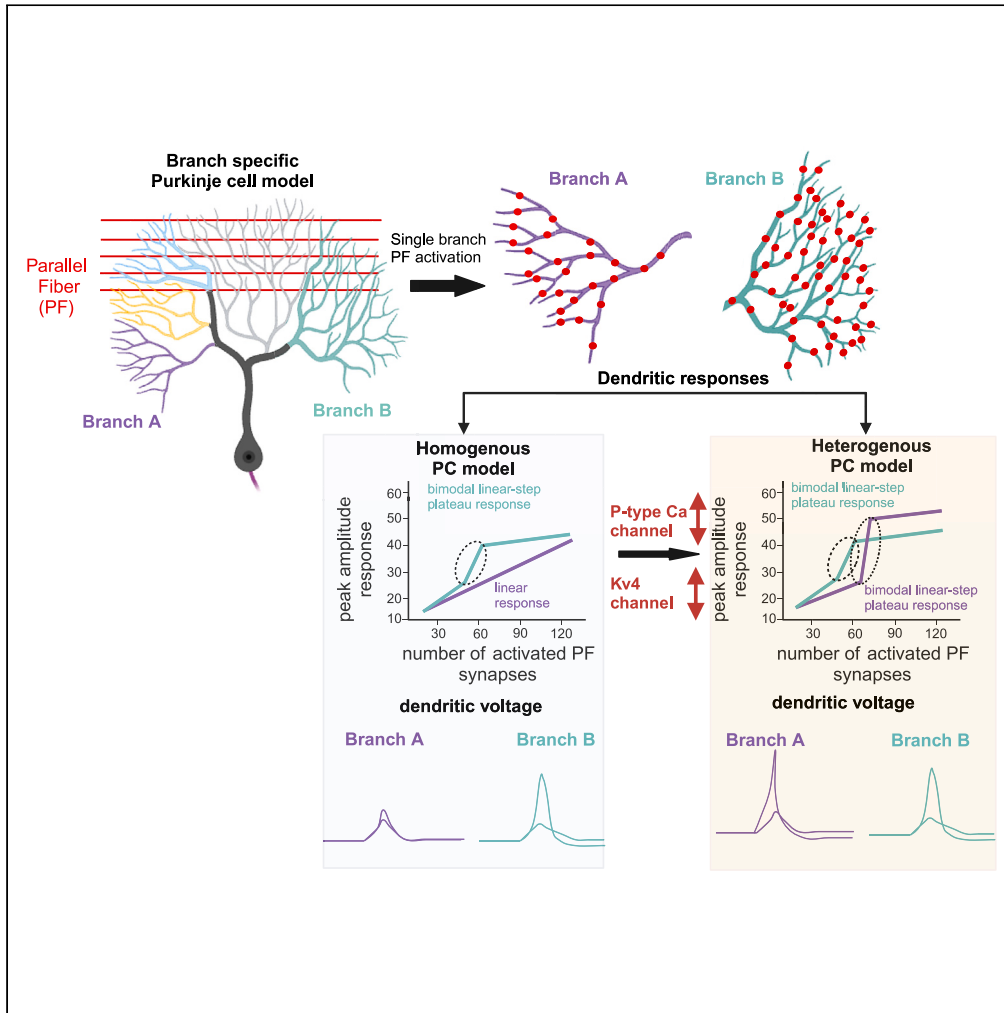


Article

Branch-specific clustered parallel fiber input controls dendritic computation in Purkinje cells



Gabriela Cirtala,
Erik De Schutter

gabriela.cirtala@gmail.com

Highlights

We propose a heterogeneous ion channel density Purkinje cell model

Branch-specific conductance densities compensate for different branch morphologies

P-type calcium channels modulate the dendritic responses at a single branch level

Increasing the conductance of Kv4.3 blocks the spreading of dendritic calcium spikes



Article

Branch-specific clustered parallel fiber input controls dendritic computation in Purkinje cells

Gabriela Cirtala^{1,2,*} and Erik De Schutter¹

SUMMARY

Most central neurons have intricately branched dendritic trees that integrate massive numbers of synaptic inputs. Intrinsic active mechanisms in dendrites can be heterogeneous and be modulated in a branch-specific way. However, it remains poorly understood how heterogeneous intrinsic properties contribute to processing of synaptic input. We propose the first computational model of the cerebellar Purkinje cell with dendritic heterogeneity, in which each branch is an individual unit and is characterized by its own set of ion channel conductance densities. When simultaneously activating a cluster of parallel fiber synapses, we measure the peak amplitude of a response and observe how changes in P-type calcium channel conductance density shift the dendritic responses from a linear one to a bimodal one including dendritic calcium spikes and vice-versa. These changes relate to the morphology of each branch. We show how dendritic calcium spikes propagate and how Kv4.3 channels block spreading depolarization to nearby branches.

INTRODUCTION

Cerebellar Purkinje cells (PCs) represent the sole output of the cerebellar cortex and are involved with encoding sensory and motor information. The extensive dendritic branching grants PCs with a unique architecture and allows them to process massive amount of information with great accuracy. PCs receive excitatory synaptic input from approximately 150,000 parallel fibers (PFs),¹ which when activated, can trigger local dendritic calcium spikes that are essential for inducing synaptic plasticity.^{2,3}

The active properties of PC dendrites were first proposed five decades ago by Llinás et al.,⁴ and ever since, the scientific community has successfully uncovered many of their properties by combining modeling and experimental studies.^{5–10} An extensive review of how PC models were first developed and their immense contribution to the understanding of the active electrical properties in the dendrites of the central nervous system was done by Bower.¹¹ It is well known that PC dendrites possess many different ion channels^{12–18} such as voltage dependent potassium channels (Kv4, Kv3), large conductance calcium-activated potassium channels (BK), small conductance calcium activated potassium channels (SK), high threshold P-type calcium channels (CaP), etc.

While PC dendritic spikes can also be generated via climbing fiber activation,^{5,19–21} in this work we will focus on the far less studied dendritic calcium spikes triggered by strong local clustered parallel fiber (PF) activation.^{2,3} During the last decade, local computation in dendrites has been captured by multiple experimental studies that highlight the importance of branch-specific generated dendritic spikes on synaptic plasticity and information storage.^{22–26} Branco et al.²⁴ discuss in detail dendritic branches acting as individual processing units, reviewing evidence of electrical, chemical, and translational compartmentalization on single branch scale, while showcasing that each branch may possess unique features given by the functional properties of its synaptic inputs. Not limited to the cerebellum, such branch-specific activity has been demonstrated in different areas of the brain like cortex^{25,26} and hippocampus.^{26,27}

In the cerebellum, Zang and De Schutter²⁸ proposed a computational model that unveiled the first evidence of localized PF dendritic spikes in a single neuron.²⁸ The authors simulated clustered PF input by randomly distributing PF synapses on 22 manually defined branches. When examining their dendritic response with respect to increasing number of PF synapses they found that four of the branches exhibited a bimodal linear-step-plateau response, characterized by a linear increase of excitatory postsynaptic potential (EPSP) amplitude until a certain threshold, followed by a voltage jump caused by a dendritic calcium spike of about constant amplitude, while most of the branches had linear responses. These interesting results suggest that single PCs are capable of implementing their own branch specific multiplexed coding.^{28,29} Moreover, this raises many exciting scientific questions such as why is the response different between branches, how does each branch-characteristic morphology affect the dendritic response and how does this influence cerebellar coding and learning capacity?

¹Computational Neuroscience Unit, Okinawa Institute of Science and Technology Graduate University, Onna 904-0412, Okinawa, Japan

²Lead contact

*Correspondence: gabriela.cirtala@gmail.com

<https://doi.org/10.1016/j.isci.2024.110756>



The well-validated model proposed by Zang and De Schutter,²⁸ like others previously developed,^{8–10,28,30–33} assumes dendritic ion channel conductance densities to be uniform throughout the PC spiny dendrite. This commonly employed assumption is traditionally made for the sake of simplicity, as considering different ion channel conductance densities would significantly increase the number of parameters used in the model and therefore the time required to properly tune these parameters. However, this common assumption may need to be reconsidered due to increasing evidence of ion channel heterogeneity across different dendrites, found in many different experimental studies in pyramidal cells^{22,23} and PCs.^{2,34–37}

In this article we propose, to our knowledge, the first heterogeneous ion channel density model in which each branch of the PC is characterized by its own set of ion channel conductance densities. We show how modifying the biophysical properties of each branch alters its peak amplitude response, producing a shift in the synaptic gain curves from linear to bimodal linear-step-plateau and vice versa. We also discuss propagation of dendritic calcium spikes within PCs, and we propose a mechanism for blocking their progression onto nearby dendrites. Additionally, we discuss how co-activation of different dendritic branches changes the gain response and dendritic spike propagation.

RESULTS

In this study, we continue the work of Zang and De Schutter²⁸ to further explore the multiplexed coding strategies that PCs use in response to a clustered PF input.^{2,3} We split the dendritic tree in 22 different branches²⁸ (Figure 1A), and we uniformly distribute PF synapses within each branch. Unlike previous literature, our model considers heterogeneous ion channel densities for each branch in the dendritic tree. In this section, we show how altering biophysical properties shifts the dendritic response from linear to bimodal linear-step-plateau and vice versa.

Role of calcium conductance density (CaP) in shifting the gain curve response

We schematically illustrate the linear versus bimodal response in the original model²⁸ in Figure 1B, where we use branch 18 to show how dendritic responses linearly increase with increasing activated PF synapses, and branch 5 for showing the bimodal linear-step-plateau response. For branch 5, we observe that initially, dendritic responses linearly increase with increasing activated PF synapses until a large “jump” is triggered (circled in Figure 1B). We define as PF threshold, the endpoint of the jump response, after which the gain curve plateaus. Figures 1C–1E show the voltage recorded at the most distal point of branch 5 (brown), branch 18 (green) and an unstimulated branch 12 for 10, 90 and 100PFs, respectively. The corresponding number of PF are simultaneously activated at t = 0ms. At the activation time, for 90PFs, we observe a relatively modest increase in both branches: 24.5mV for branch 5 and 21.6mV for branch 18. However, for 100PFs, we observe in Figure 1E a large increase of 41.2mV for branch 5, while branch 18 only shows a modest 24.4mV rise. This sharp increase for branch 5 gives the 15mV “jump” shown in Figure 1B. Observe that the dendritic response corresponding to the unstimulated branch 12 remains the same regardless of the PF increase. Figures 1F–1H show the response at soma for the same number of PFs, for branch 5 (brown) and branch 18 (green, dotted). Notice that as the PF number increases, after the PF activation, the somatic spikes corresponding to the two branches occur at different times. In Figure 1H we also observe a somatic burst for branch 5 after activation of PF input.

To illustrate how altering the biophysical properties of the PC can result in a change in the synaptic gain curve, we use two different branches with distinct behaviors: branch 3 (see Figure 2), for which the dendritic response increases linearly with PF stimulation, and branch 15 (see Figure 3), which already exhibits a bimodal response. For these two branches, we show how the dendritic response changes when altering the CaP conductance densities (CaP_g) and we analyze how the dendritic spikes propagate.

Figure 2A shows the morphology of branch 3 on which we uniformly distributed 2 to 200 PF synapses with a step of 2PF. We selected two points: a distal point p_1 and a proximal point p_2 , in which we recorded the voltage and calculated the dendritic responses with respect to the number of activated PFs. The black line in Figure 2B, shows the linear response obtained when using the original uniform ion channel density model.²⁸

We gradually increased the CaP_g for the spiny dendrites in branch 3 by 30% (magenta), 50% (blue) and 70% (red). We observed that a 70% increase is sufficient to shift the response from linear to bimodal linear-step-plateau. The “jump” is initiated at 46PF and reaches its plateau at a threshold of 48PF, shown with a black star in Figure 2D, and has a peak amplitude difference of 11mV. Unlike the distal point, the dendritic response at the proximal point p_2 (Figure 2C) shows a very small increase when activating the PF input. Figures 2D–2I considers an increase of 70% in CaP_g.

In Figures 2E and 2F, we visualize the shape of the voltage recorded at the distal point p_1 , and at the proximal point p_2 for different number of activated PF synapses. In our simulations, the PC fires spontaneously, as observed experimentally,³⁸ and we activate the PF input at time t = 0ms as indicated in the red marker. In Figure 2E, we observe that activating a sufficiently large number of PF synapses, produces a transition from EPSP to large amplitude dendritic spike when recording the voltage in p_1 . On the other hand, the voltage recordings at the proximal point p_2 show no significant depolarization (Figure 2F).

Figures 2G–2I show the dendritic spike propagation when activating 48PFs on branch 3. At 1ms after activation, we observe a very small depolarization starting at the tip of branch 3 and propagating toward the smooth dendrite (see Figure 2G). This depolarization increases as the time passes and reaches its maximum depolarization of -17mV after 3ms (see Figure 2I). This depolarization remains entirely local and does not spread to any of the nearby branches. The video of the dendritic spike propagation is available as online Video S1.

When examining a much larger branch such as branch 15 (see Figure 3), we observe a different behavior. This branch already exhibited a bimodal linear-step-plateau response, but it was not reported in the previous analysis²⁸ due to its very large threshold at which the “jump” occurs (see black line in Figure 3B), which exceeded the maximum number of PFs considered.²⁸ We use this branch as an example of how the

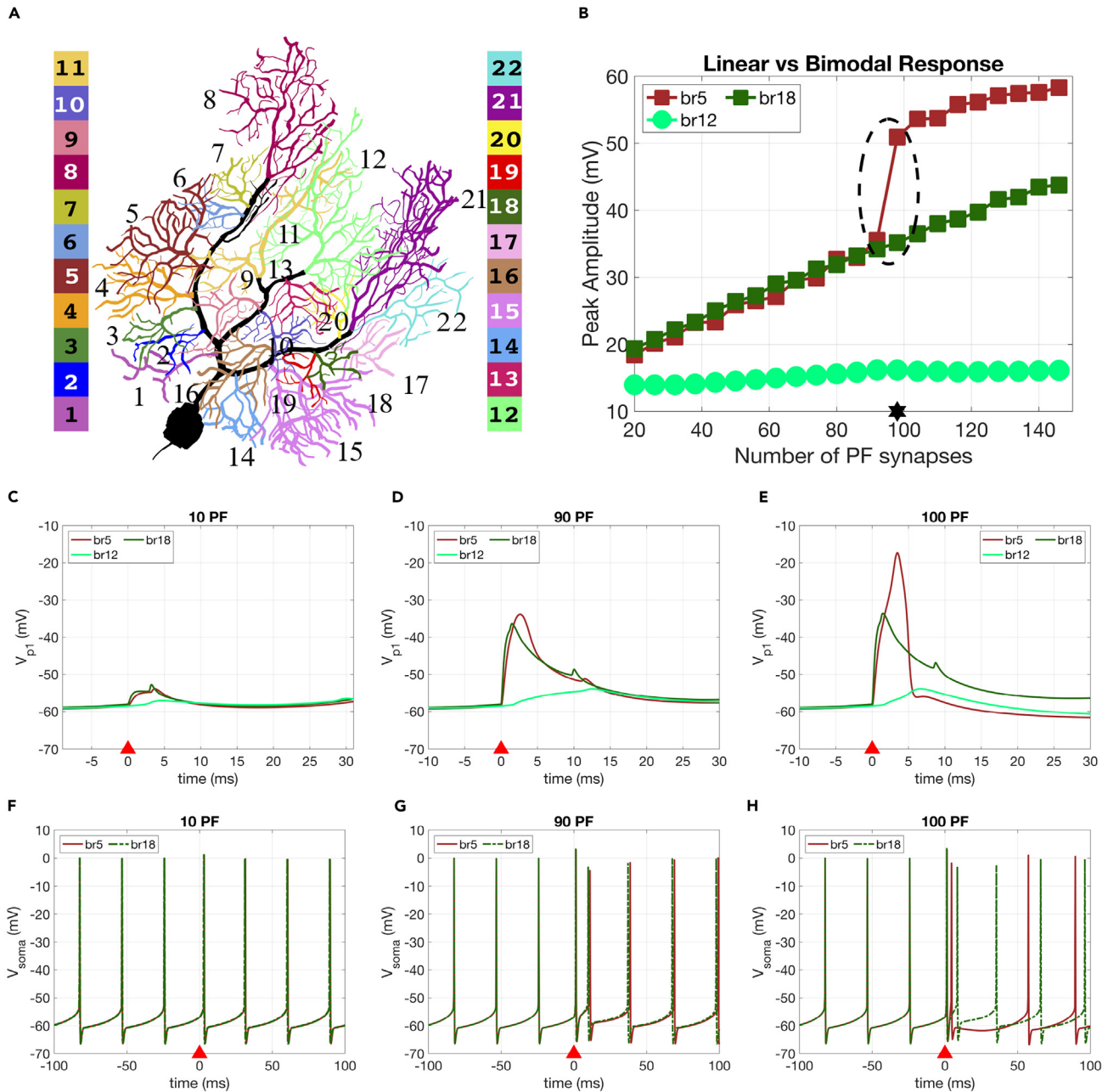


Figure 1. Examples of linear and bimodal responses for different dendritic branches

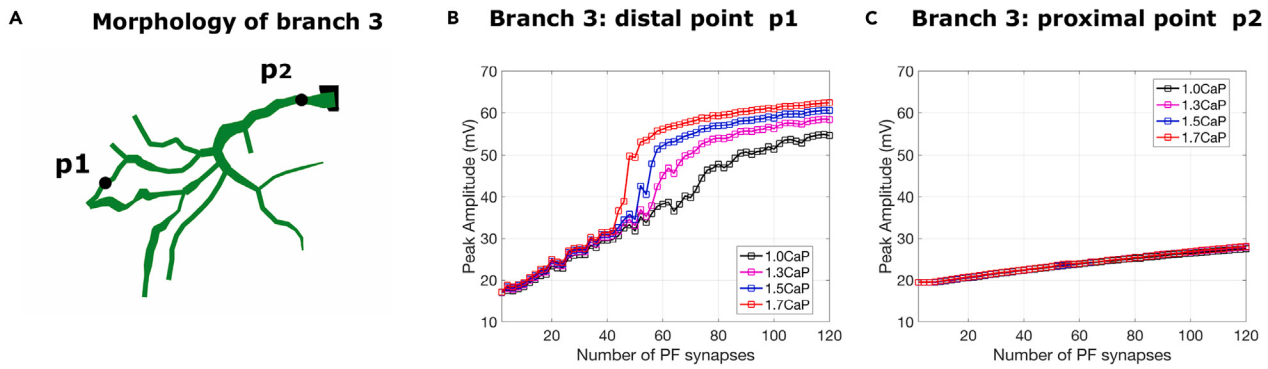
(A) Branches of the Purkinje cell model. The spiny dendrites were grouped into 22 branches, such that each branch connects to the smooth dendrite shown in the thick black line.

(B) Dendritic responses with respect to increasing number of activated PF synapses: bimodal linear-step-plateau response for branch 5 (brown) and linear response for branch 18 (green). Additionally, we show the response in the unstimulated branch 12. Branch 5 is characterized by an initial linear response, followed by a step increase in the gain curve. The “jump” in the peak amplitude is 15mV, occurs for a number of 94 activated PF and is followed by another linear response once the threshold of 96PF is reached.

(C-E) Voltage responses recorded at the distal point of branch 5 (red), branch 18 (green) and the unstimulated branch 12 (light green), for different PF numbers: 10PF (panel C), 90PF (panel D) and 100PF (panel E). The response in branch 5 to 100 activated PFs shows a dendritic calcium spike is triggered.

(F-H) Voltage responses recorded at soma for 10 PF (panel F), 90PF (panel G) and 100PF (panel H).

bimodal response can in turn be converted to a linear response by reducing the CaP_g . In Figures 3B and 3C we show the response for the baseline value of 1.0CaP_g used²⁸ and we show that even a reduction of 20% of CaP_g conserves the bimodal response (magenta line). However, if we reduce this further by 40%, it shifts to a linear response (blue line).



Results for 1.7CaP

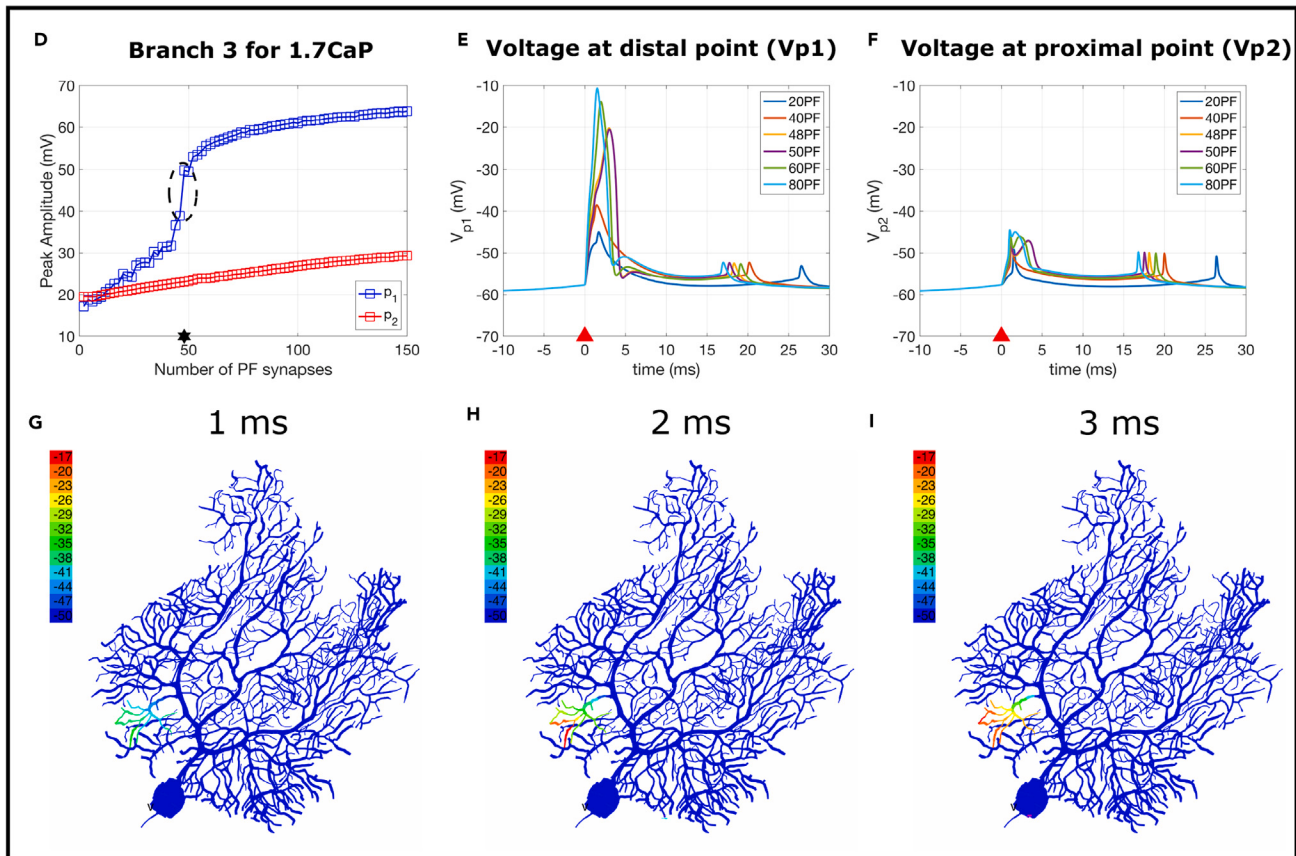


Figure 2. Increasing CaP_g converts the dendritic response from linear to bimodal: example branch 3

(A) Illustration of branch 3. The voltage is measured at two points: distal point p_1 and proximal point p_2 .
(B and C) Dendritic responses for the distal point p_1 and the proximal point p_2 , respectively with increasing number of activated PF synapses. The black line indicates the response when considering the reference value of P-type calcium channel conductance density (CaP_g), while the magenta, blue and red lines show relative increases in P-type calcium channel conductance density of 30%, 50%, respectively 70%.
(D) Dendritic responses for the two points p_1 and p_2 for an increase of 70% in CaP_g . The bimodal linear-step-plateau response (circled) occurs at a threshold of 48PF (shown using a star).
(E and F) Voltage response measured at the point p_1 and p_2 for different number of activated PF in [2,120] for the case of 70% increase in CaP_g . The smaller spikelets at the end of each recording are attenuated somatic action potentials.
(G–I) Dendritic spike propagation after 1ms, 2ms and 3ms from activating the PF input. Observe that the dendritic spikes initiate at the tip of branch 3 and propagate toward the smooth dendrite, depolarizing the entire branch. This depolarization is entirely localized, no spreading to neighboring branches is observed.

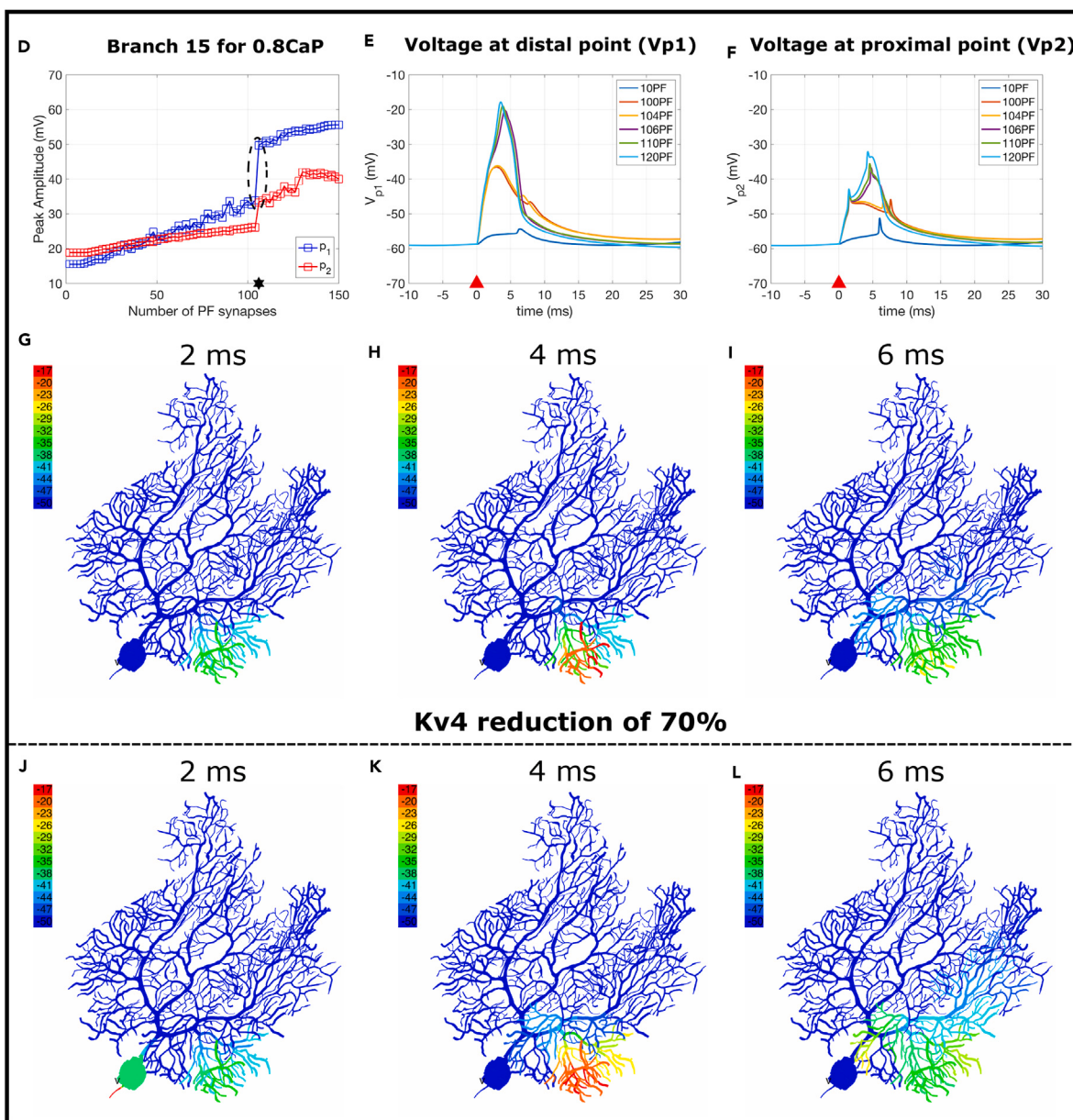
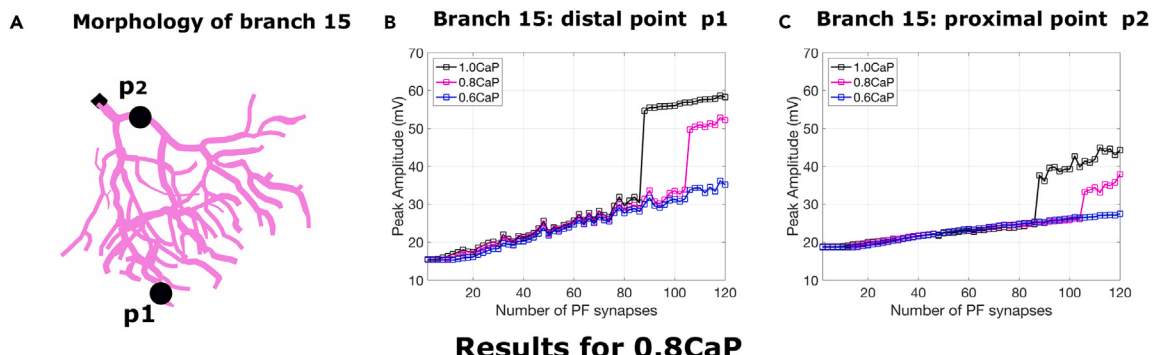


Figure 3. Decreasing CaP_g converts the dendritic response from bimodal to linear: example branch 15

- (A) Illustration of branch 15. The voltage is measured at two points: distal point p_1 and proximal point p_2 .
- (B and C) Dendritic responses for the distal point p_1 and the proximal point p_2 , respectively with increasing number of activated PF synapses. The black line indicates the response for the reference value of CaP_g, while the magenta and blue lines show relative decreases in CaP_g of 20% and 40% respectively.
- (D) Dendritic responses for the points p_1 and p_2 for a decrease of 20% in CaP_g. The bimodal linear-step-plateau response (circled) corresponds to a threshold of 106 PF (black star).
- (E and F) Voltage response measured at the point p_1 and p_2 for different number of activated PFs in [10,120] for the case of 20% decrease in CaP_g.
- (G–I) Dendritic spike propagation 2ms, 4ms and 6ms after activating the PF input. Observe that the dendritic spikes initiate at the tip of branch 15 and propagate toward the smooth dendrite, depolarizing the entire branch. In panel I we observe that there is a small depolarization of -41mV of the neighboring branch 14.
- (J–L) Dendritic spike propagation when decreasing Kv4.3 conductance density by 70% in addition to the 20% CaP reduction.

In panels D–I we show the results obtained for a reduction of 20% in CaP_g. This reduction limits the depolarization onto the neighboring branches, while maintaining the bimodal response circled in Figure 3D, where we observe a very large threshold of 106PF. When examining the dendritic responses in the distal point p_1 , we observe a very large "jump" of 15.8mV, while in the proximal point p_2 , we have a very modest "jump" of 7.2mV.

The dendritic spike propagation in branch 15 is shown in Figures 3G–3I where we activated 106PF. Two ms after activation we observe a small depolarization which starts on the tip of branch 15 and propagates toward the smooth dendrite (see Figure 3G). The depolarization increases further and reaches its maximum after approximately 4ms (see Figure 3H). In Figure 3I we show how, after 6ms from activation, the depolarization minimally spreads to the neighboring branch 16, where it reaches a maximum of -41mV (see Video S3). On the other hand, in Figure 3J–3L we observe the dendritic spikes when the Kv4.3 conductance density is reduced by 70%. Observe that the dendritic spike propagation becomes more pronounced, encompassing not only neighboring branch 16, but also more distal branches 17–21. A previous Ca^{2+} imaging study that demonstrated Kv4.3 channel expression in PC dendrites¹⁸ supports our idea. We will describe in more detail the effect of Kv4.3 on dendritic spike propagation in the next section.

Role of Kv4.3 in blocking the depolarization to nearby branches

The work of Zang and De Schutter²⁸ shows that activating clustered PF on branch 8, one of the largest and most distal branches of the PC, produces a very large depolarization onto the nearby much smaller branches 6 and 7. We investigated various modalities of constraining such depolarizations. Our first attempt was to reduce the CaP_g as shown in the previous section. This strategy can indeed decrease the depolarization (see Video S1), however, reducing CaP_g by more than 10% in the case of branch 8 results in a shift of the dendritic response from bimodal to linear.

Therefore, to limit the depolarization while maintaining a bimodal linear-step-plateau response, we investigated the role of the voltage-activated potassium channel, Kv4.3. We observed that by increasing Kv4.3 conductance densities (Kv4.3_g) on the larger branches and nearby smaller branches, we were able to significantly reduce the spreading (see Video S4 and S5). Contrarily, decreasing Kv4.3_g by 70% for branch 15 led to much more significant depolarizations on the nearby branches 16–21 (see Figures 3J–3L), while on smaller sized branches such as branch 3 or branch 10 (see Figures S4J–S4L) decreasing Kv4.3 did not produce any spreading depolarization onto neighboring branches but did slightly affect the timing of the depolarization (see Figure S4K).

Figures 4D–4F shows the dendritic spike propagation for branch 8 when increasing Kv4.3_g on branch 8, 7 and 6. Notice that in this case, the dendritic spikes propagate throughout branch 8 and they only slightly spread toward branches 6 and 7 (-44mV) (see Video S5).

Similar behavior was observed for branch 7 (Figures 4G–4I). When activating PF on branch 7, we notice that the dendritic spikes propagate throughout the entire branch (Figure 4G) and fully depolarize the neighboring branch 6 (Figure 4H), after which they spread toward branch 8, provoking a full depolarization (Figure 4I). On the other hand, when increasing Kv4.3_g (Figure 4J–4L), we observed that the dendritic spikes initiating in branch 7 (Figure 4J) are entirely constrained within the same branch (Figure 4L). The videos are available in the Video S4.

When examining the entire dendritic tree, we determined that for most branches, the dendritic spikes are entirely constrained within the branch in which they originate, as shown in experimental work by Vetter et al.³⁹ For the branches which exhibited large depolarizations (such as branches 5, 6, 7, 8, 11, 12, 13), we adjusted the Kv4.3_g so that the voltage stayed below -35mV on the nearby branches. All Kv4.3_g changes are summarized in Figure 5D.

We identified two outlying branches whose spreading depolarization could not be fully constrained: branch 12 and branch 18 (see Video S2 and S3). For branch 12 (see Figure S6), we were only partially successful in blocking the depolarization toward the nearby branches 9, 10, 11 and 13. We believe this is due to the special morphology of branch 12, a very large and distal branch located on the center part of the dendritic tree. By adjusting the Kv4.3_g on branch 11, 12 and 13, we were able to limit the depolarization toward branch 12, when activating branch 11 and branch 13. However, when activating PF on branch 12, the spreading depolarization first reaches branch 13 and 11, after which it continues toward branch 9 and 10. We included the results for branch 12 in the supplemental information (see Video S2 and Figure S6). On the other hand, branch 18 is the smallest branch in our PC (see Figure 6A) and is located in the immediate vicinity of branch 19, being connected to the same smooth dendrite. We believe its morphology, and its close proximity to branch 19 (see Figure S2), makes it impossible to contain the depolarization toward its neighboring branches 19 and 17.

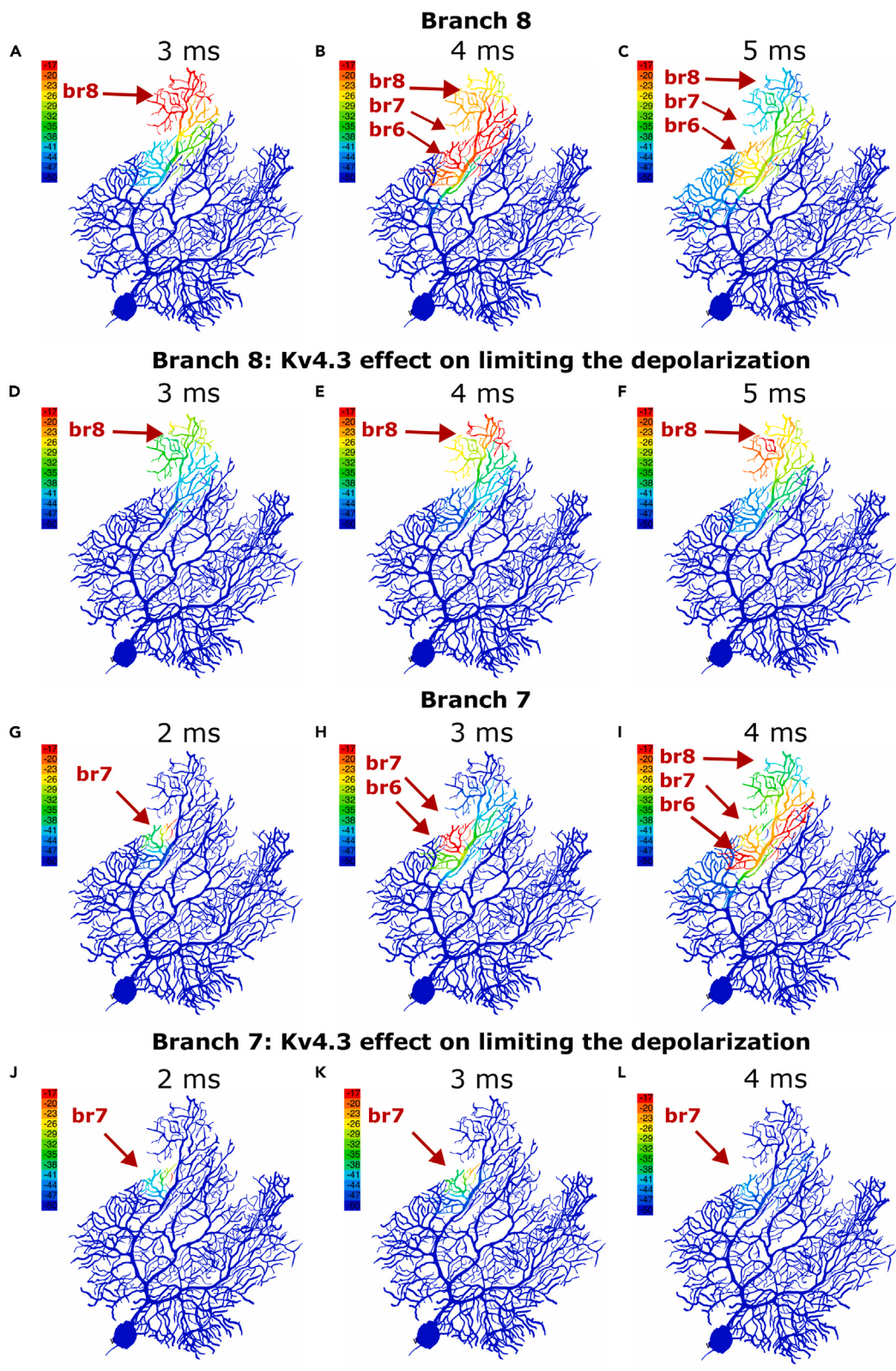


Figure 4. Role of the voltage dependent potassium Kv4.3 channel in blocking depolarization of nearby branches

(A–C) Dendritic spike propagation for branch 8 when CaP_g is reduced by 10%. Observe that activating PF on branch 8 produces a very strong depolarization on the smaller neighboring branches 6 and 7.

(D–F) Dendritic spike propagation for branch 8 when increasing Kv4.3_g by 1.9-fold for branch 5, 2.2-fold for branch 6, 2.6-fold for branch 7 and 2.2-fold for branch 8. Compared to the previous row (A–C), the spreading onto the nearby branches is significantly reduced.

(G–I) Dendritic spike propagation for branch 7. Observe that the dendritic spikes propagate first toward branch 6 and then toward the entire branch 8.

(J–L) Dendritic spike propagation for branch 7 with same changes to Kv4_g as in panels D–F. Notice that the dendritic spikes are entirely constrained to branch 7.

Summary of the results obtained for each branch

Following the same algorithm for each branch in the dendritic tree, we were able to convert the response from linear to bimodal linear-step-plateau for all branches. We summarize the results obtained in [Figure 5](#), where in panel A we show the response when considering the original uniform channel density model,²⁸ while in panel B we show the bimodal response obtained with our novel heterogeneous ion channel density model. Panel A shows in gray all the branches characterized by a linear response and in color, the branches that already showed a bimodal response: in squared markers we indicated the four branches that were captured in previous work,²⁸ while in circle markers we show the branches that were overlooked. All our simulations were performed for a maximum of 200PF for all individually activated branches, but as no further jumps were detected after the threshold of 106PF, in [Figures 5A](#) and [5B](#) we show the response till 150PF. The color coding used in all the graphs follows the same color scheme chosen in [Figure 1A](#).

The modifications we made to the CaP and the Kv4.3 channel densities for each branch are collected in [Figures 5C](#) and [5D](#) and are expressed as relative changes with respect to the baseline values (see [Table S1](#)). We correlate the values of the ion channel conductance densities to various morphological properties of the corresponding branch such as length and distance from soma in Section [morphological factors that influence branch excitability](#). All the results we show in the rest of this paper follow the parameter choices shown in [Figures 5C](#) and [5D](#). Observe that each branch has a characteristic PF threshold, which we define as the finish point of the “jump” and the starting point of the plateau. We collected these values in [Figure 5E](#), where we observe that the thresholds vary significantly between 22PF for branch 22 to 106PF for branch 15, with an average value of 59PF, expressed by the dash-dotted line in panel E.

In conclusion, in this section, we presented the results obtained when simulating a clustered PF input^{2,3} on each branch of the PC. Our model employing branch-specific conductance densities compensates for the different branch morphologies and achieves a uniform bimodal linear-step-plateau response throughout the PC. In addition, our model fully or partially constrains dendritic calcium spike propagation within the activated branch. In these simulations, our PC fires spontaneously at 34 Hz, which corresponds to the firing frequency of PCs located in the zebrin-positive (Z+) module discovered by the experimental work of Zhou et al.⁴⁰ to be 36 ± 15.5 Hz. For PCs corresponding to the zebrin-negative (Z-) module, which fire at a much higher frequency of 76 ± 19.5 Hz, we show the results in the [supplemental information](#) ([Figure S7](#)). We observed that for the higher excitability case, nearly half of the branches already exhibit a bimodal response when CaP is maintained at its reference value. For the remainder of the branches, we show that the CaP increases required to achieve bimodal responses (see [Figure S7C](#)) are significantly smaller compared to the Z+ results shown in [Figure 5C](#).

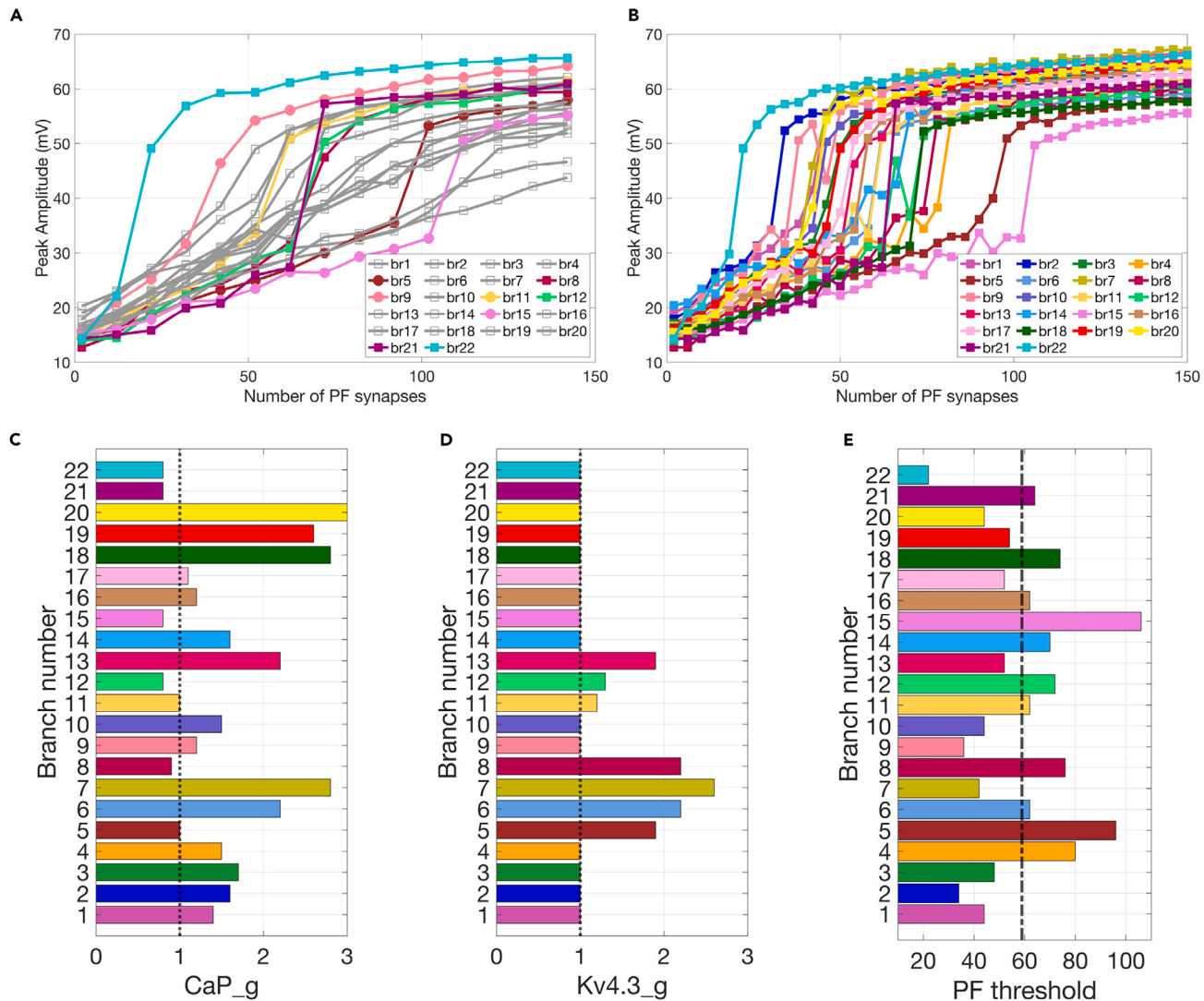
Basic properties of the heterogeneous densities model

In response to climbing fiber input, our novel heterogeneous PC model generates complex spikes as shown in [Figure S7E](#) for the Z+ case and [Figure S7F](#) for the Z-case. Notice that the pause following the complex spike for the Z+ case is considerably larger than the pause recorded for Z-, which is in agreement with experimental work.⁴⁰ In addition, we show the frequency-current curve, obtained when injecting different current amplitudes at soma in [Figure S7G](#). The results we obtained using the heterogeneous ion channel density model (red line in [Figure S7G](#)) are similar to the F-I curve of the homogeneous model²⁸ (blue line). Both F-I curves fall in the experimentally measured range (see [Figure 1F](#) from Zang et al.³³).

Quantitative analysis of dendritic calcium spikes

Our simulations capture how strong enough clustered PF input on each branch of the PC, initiate dendritic spikes. [Figures 2G–2I](#), [3G–3I](#), and [4](#) show how the dendritic spikes initiate at the tip of the stimulated branch/branches and propagate toward the smooth dendrite. As they reach the smooth dendrite, their amplitude decreases, as observed experimentally.^{2,3} For most branches in the dendritic tree, the dendritic spikes are either entirely spatially constrained or they provoke minimum depolarization on the nearby branches. The only exceptions are the larger more distal branches such as branch 8 ([Figure 4](#)) or branch 12 ([Figure S6](#)), which strongly depolarize the neighboring much smaller branches 7 and 6 ([Figures 4A–4C](#) and [4G–4I](#)), respectively 11 and 13 ([Figure S6](#)). This depolarization, which was already captured in the previous work,²⁸ was blocked by increasing Kv4.3 conductance density (see [Figures 4D–4F](#) and [4J–4L](#)) as summarized in [Figure 5](#). Following these modifications, most dendritic spikes remain local within the branch they originate from or, in some instances, provoke minimum depolarization on the nearby branches. However, there are two exceptions (branch 12 and 18) for which our heterogeneous model was not fully able to compensate for the distinct morphology of these branches and the propagation of the spikes could be only partially reduced.

We observed that the time required to achieve maximum depolarization is highly dependent on the branch considered, varying from 2 to 3ms for the small branches situated near the soma such as branch 3 ([Figure 2](#)), 10 ([Figure S4](#)) to 5-8ms for the larger more distal branches such as branch 5 ([Figure S3](#)), 8 ([Figure 4](#)), 11 ([Figure S5](#)) or 12 ([Figure S6](#)).

**Figure 5. Results and parameters for the heterogeneous model**

(A and B) Dendritic responses using the homogeneous ion channel model (A) or the heterogeneous ion density channel model (B). The branches shown in gray in panel A exhibit a linear response when simulated using the homogeneous model. The branches shown in colors show a bimodal response: branches 8, 12, 21, and 22 (squared markers) were already shown to have a bimodal response²⁸ while branches 5, 11, and 15 (circle markers) were overlooked in the previous work due to their very large PF thresholds. Panel B shows that all branches exhibit a bimodal response, when using our heterogeneous ion channel model.

(C and D) Relative changes in ion channel densities for obtaining the bimodal response for all the branches for CaP_g (panel C) and Kv4.3_g (panel D). The dotted lines indicate the baseline conductance densities used in the homogeneous model.

(E) The minimum number of PF required within each branch for initiating the jump. The dashed-dotted line indicates the average threshold.

Morphological factors that influence branch excitability

One possible factor that may control the excitability of each branch is its length. In Figure 6A we show the cumulative lengths of all branches in our dendritic tree. We observe that the more distal branches (8, 12 and 21) also have the largest lengths. When correlating the PF thresholds with the length of each branch and the distance from soma, a moderate statistical correlation was found: a positive Pearson correlation coefficient of 0.467 with a *p* value of 0.028. The correlation between the PF thresholds and the distance to soma was insignificant (Pearson correlation coefficient 0.0483, *p* value 0.8309).

One other factor that controls the excitability within each branch is the P-type channel conductance density. In order to convert the linear response into a bimodal one, we increased the conductance density of the P-type calcium channels for the spiny dendrites as summarized in Figure 5C. Additionally, we show the distribution of CaP conductance densities across the dendritic tree in Figure 6D. The color bar indicates the relative increase with respect to the baseline value. As described in the previous sections, the most distal branches such as branch 8, 12, 21 and 22 already exhibited a bimodal response. The CaP_g was lowered to 90% of its value for branch 8 and 80% of its value in case of branches

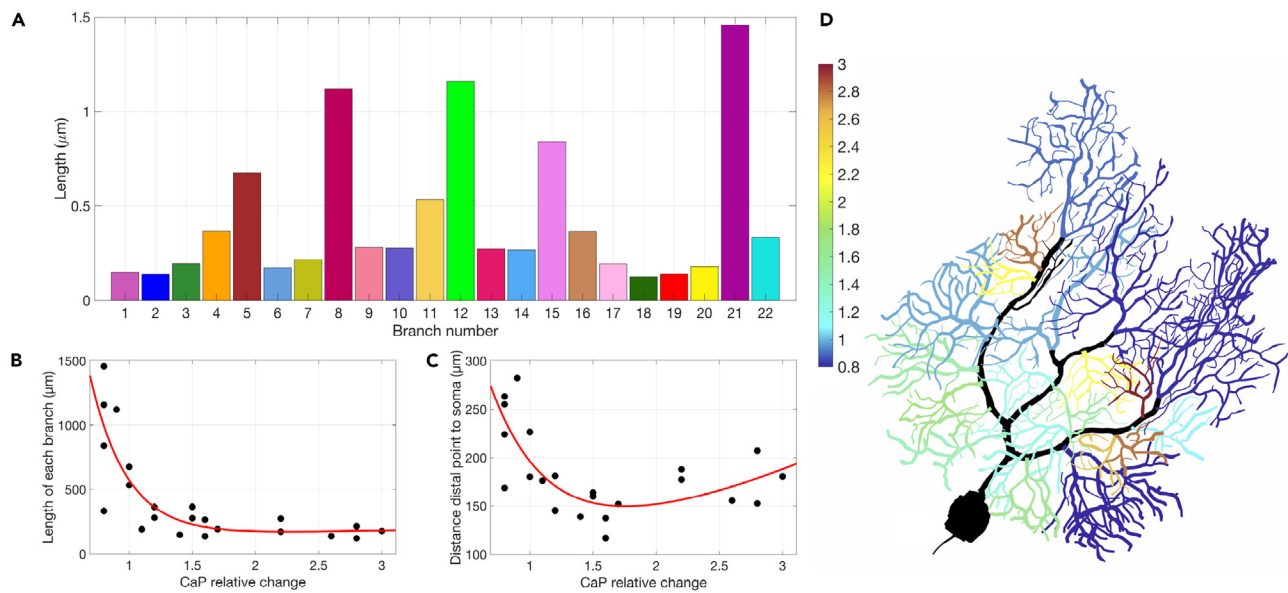


Figure 6. Morphological properties of the branches

- (A) Cumulative lengths of each branch in the PC.
- (B) Scatterplots for the relative change in CaP_g and the length of each branch, which were fitted with a sum of exponentials (in red).
- (C) Scatterplots of the relative change in CaP_g and the distance from the most distal point of each branch to the soma, fitted with a sum of exponentials (in red). In the first case the R^2 obtained is 0.6214, while the second one has a R^2 of 0.5542.
- (D) Distribution of relative increase in CaP_g required for obtaining a bimodal response for all branches.

12, 21 and 22 to limit the dendritic spike propagation from these branches to the nearby branches. Moreover, the relatively large branches such as branch 5 and 11 required no increase in CaP_g. On the other hand, very small branches such as branches 18, 19 and 20 needed a very large increase in CaP_g of 2.8, 2.6, respectively 3-fold of the baseline value.

Following these observations, we analyzed the statistical correlation between the increases in CaP_g required for obtaining bimodal response and two parameters: the cumulative length of each branch (see Figure 6A) and the distance between the distal point at each branch and the PC soma. The length of each branch and the CaP_g relative increase were strongly negatively correlated (Pearson correlation coefficient -0.6246 , p value 0.0019). In other words, the larger the branch size, the smaller the relative CaP_g increase needed to obtain the bimodal response. When examining the distance from the distal point of each branch to the soma and the relative CaP_g increase, we obtained a Pearson correlation coefficient of -0.3761 with a p value of 0.084. This moderate negative correlation implies that shorter distances to the soma require larger CaP_g relative increases. Figures 6B and 6C show scatterplots for the CaP_g relative change with respect to the length and the distance to soma, respectively.

The analysis indicates that the length of each branch is moderately correlated with the PF threshold but highly correlated with the CaP_g increase required for achieving a bimodal linear-step-plateau response.

Multiple branch activation

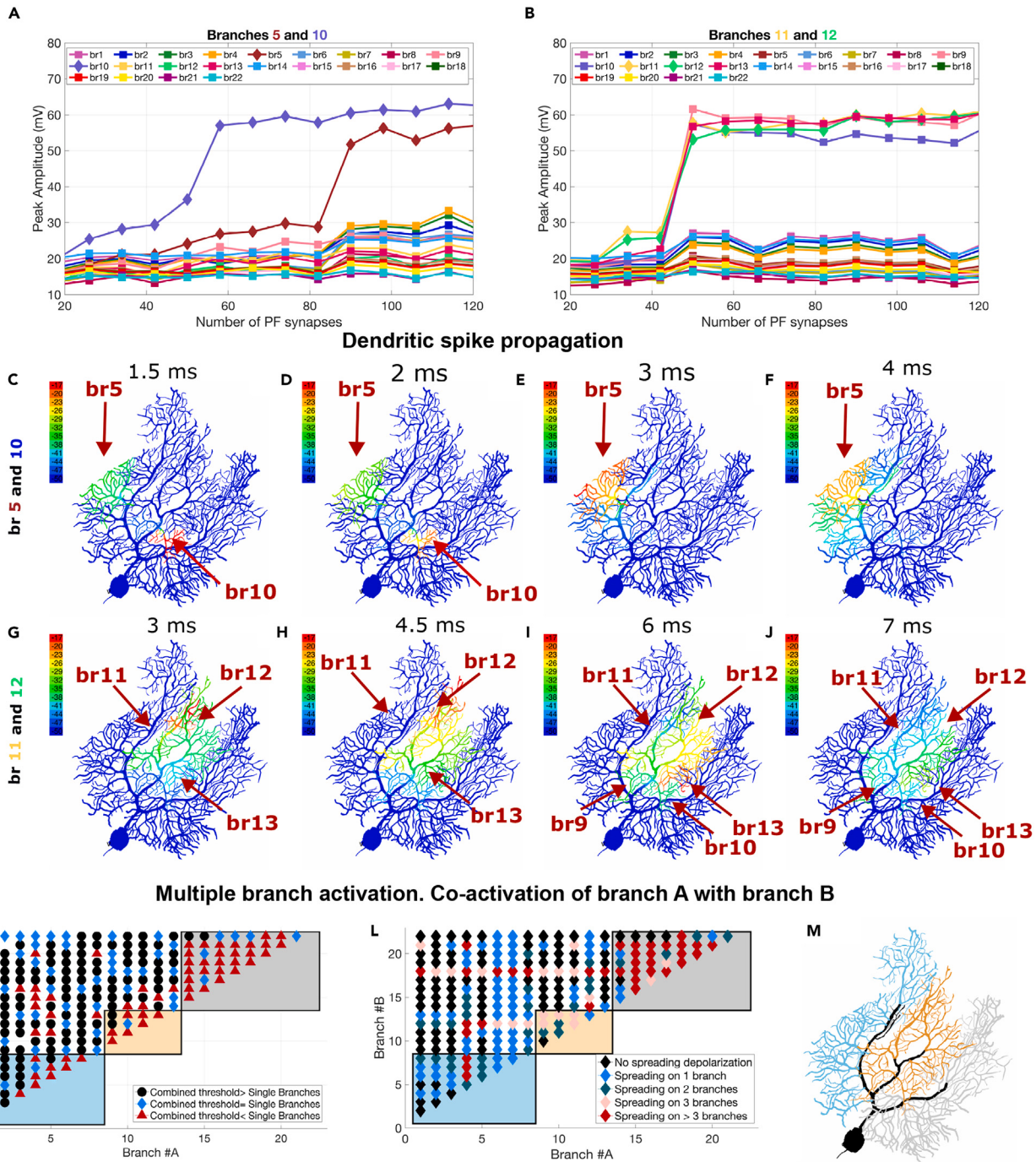
We simulated co-activation of clustered PF input on two branches, and we analyzed the dendritic responses and the propagation of the dendritic spikes. In Figures 7A–7J we show two different examples of co-activated branches, while in Figures 7K and 7L we describe the results obtained for all possible branch combinations.

In Figure 7A we activated clustered PF input on two branches: branch 5, located on the left part of the dendritic tree and branch 10, located on the middle part of the tree. We uniformly distributed 20 to 120PF on each of the two branches. In Figure 7A we observe that the bimodal response is maintained for the two activated branches, while the remainder of the branches show no increase in their peak amplitude. When simultaneously activated, branch 5 reaches its step response for a threshold of 90PF, while branch 10 only requires 58PF. These PF thresholds are very similar to those obtained when individually activating each branch: 96PF for branch 5 and 44PF for branch 10 (see Figures S3 and S4).

The local activation of the two branches can be better seen in Figures 7C–7F, where we visualize the dendritic spikes which initiate at the tip of each branch, propagate within these branches, and achieve maximum depolarization in Figure 7C for branch 10, after only 1.5ms from activation and in Figure 7E for branch 5, which requires approximately 3ms. In Figure 7F we see a very small depolarization produced by branch 5 onto its neighboring branches 4 and 3, while the dendritic spikes originating in branch 10 remain entirely constrained.

Figure 7B shows the co-activation of branches 11 and 12, two neighboring branches located on the distal middle section of the PC (see Figure 1A). Unlike the previous branch combination shown in Figure 7A, we see that once the threshold of 50PF is reached, a large “jump”

Examples of multiple branch activation

**Figure 7. Multiple branch activation**

(A and B) Dendritic responses for simultaneous activation of PF input on branches 5 and 10 (panel A) and branches 11 and 12 (panel B), respectively. In both cases, we observe that the bimodal response is maintained for the activated branches marked with diamond markers. When co-activating branch 5 and 10, the remainder of the branches exhibit a linear response (squared markers), while when co-activating branches 11 and 12, there is a strong bimodal response in neighboring branches 9, 10, and 13.

(Panels C–F) show the dendritic spike propagation for simultaneous activation of branches 5 and 10, while panels G–J show the dendritic spike propagation for branches 11 and 12. Observe that for the first example, the dendritic spikes remain localized in the branch they originated from, showing a very small

Figure 7. Continued

depolarization onto branches 3 and 4 at 4ms (panel F) of approximately -38mV and -41mV . On the other hand, the second case shows a large depolarization (-17mV) on the entire middle part of the dendritic tree (panels I and J).

(K) Comparison between PF thresholds for individually activated branches versus co-activated branches. Black markers correspond to at least one of the co-activated branch PF thresholds being larger than that for the individually activated branch, blue markers imply equality while the dark red marker shows that the combined branch threshold is smaller than the PF threshold of the single branch.

(L) Assessment of spreading depolarizations when co-activating different branches. For each pair of co-activating branches, colored markers show how many additional branches have a spreading depolarization that is larger than -35mV .

(M) Main branch divisions of the PC: left division (light blue), middle division (orange) and right division (gray). The colored rectangles in panels K and L indicate that the branch combinations belong to the same main division defined in panel M.

occurs not only for branches 11 and 12 but also their neighboring branches 9, 10 and 13. This threshold is significantly smaller than the scenario in which the two branches are individually activated: 62PF for branch 11 (Figure S5) and 72PF for branch 12 (Figure S6).

Figures 7G–7J show the dendritic spike propagation when co-activating branch 11 and 12. We observe how initially branches 11 and 12 are activated, after which the depolarization spreads on the lower branches 9, 11 and 13, where it reaches -17mV . The co-activation of branches 11 and 12 is one of the most extreme scenarios in our analysis, in which dendritic spikes spread on the entire middle main branch. We believe this occurs due to the very close proximity of the two branches (see Figure S2), their large sizes (see Figure 6A), and their more distal positions.

Figures 7A and 7B show two opposite examples of multiple branch co-activation. In order to examine the responses in the entire dendritic tree, we analyzed all possible two by two branch co-activations and we performed two sets of tests (Figures 7K and 7L). To ease the description of the results, we show in Figure 7M three main divisions of the PC: the left most main division (in light blue), the middle main division (in orange) and the right main division (in gray). The squared rectangles colored in light blue, orange and gray, respectively in Figures 7K and 7L indicate co-activated branches that belong to the same main division.

First, we compared the threshold for co-activation of the two branches with the thresholds of individually activated branches. We observed that for most of the tree, the co-activated branch thresholds are larger or equal than the threshold of the single branches (black and blue markers in Figure 7K). For example, the co-activation of branches 5 and 10 (see Figure 7A) corresponds to this case. However, when activating nearby branches or branches belonging to the same main division (indicated in the colored rectangles in Figure 7K), due to the spreading depolarizations between the two branches and to the surrounding branches, the combined threshold becomes smaller than the individually activated branch threshold (dark red markers in Figure 7K). The extreme scenario of branch 11 and 12 described above corresponds to this second case. In conclusion, the branches act as individual processing units if they are well separated from each other, ideally located on different main divisions. The closer the co-activated branches are to each other, the smaller their PF threshold becomes, and they no longer function as individual units.

Second, for all possible branch combinations, we studied how their dendritic spikes propagate. In Figure 7L we show whether their dendritic spikes remain local, or they spread toward the neighboring branches. In case of spreading depolarization, we counted how many neighboring branches show a voltage larger than a set threshold value of -35mV . The black diamond symbol in Figure 7L shows no spreading depolarization, while the dark red marker shows that the depolarization is detected in more than 3 branches. While most of the dendritic tree shows no significant depolarization, there are few exceptions that stand out. Firstly, branch 6 co-activated with any other branch (blue diamond marker), results in a depolarization of its neighboring branch 7. Conversely, branch 7 triggers a depolarization on branch 6. This suggests that these two very small branches that are extremely close to each other (see Figure S2) are intertwined and could be redefined as a single branch. The same occurs with branch 18 and 19, the smallest branches of the PC (see Figure 6A), which are also very close. As we discussed in Section [role of Kv4.3 in blocking the depolarization to nearby branches](#), we were unsuccessful in containing the spreading depolarization when individually activating branch 18, as it contacted its close neighbor branch 19 and further spread on the right main division. Here, when co-activating branch 18 with any of the branches in the PC, we observed more extreme depolarizations. Also, significant depolarizations occur when co-activating branches from the center main division (orange rectangle), because, as soon as branch 12 is co-activated with any other branch, there is significant depolarization on its neighboring branch 11 and 13. This was also discussed in Section [role of Kv4.3 in blocking the depolarization to nearby branches](#) and in the Figure S6, in which we show how the dendritic spikes propagate when activating PF only on branch 12. Of course, the dendritic calcium spikes originating in this branch, when co-activated with any other branch, trigger stronger depolarizations.

Note that for this analysis, we maintained the same Kv4.3_g parameter choice as defined in Figure 5D and Table S2. Further increasing Kv4.3_g for the co-activated branches could possibly have a significant effect in reducing these depolarizations. However, our interest here was to determine whether these branches can function as individual units, based on morphological criteria.

DISCUSSION

Building the first heterogeneous ion channel density model

In vitro studies have shown that dendritic calcium spikes can be triggered by clustered PF input.^{2,3} These dendritic spikes are caused by the activation of dendritic voltage-gated calcium channels. Confirmation of their study *in vivo* has been very challenging using conventional patch-clamp recordings, but recently, with the development of techniques such as *in vivo* calcium imaging, various authors recorded PF evoked dendritic spikes.^{41–45} In particular, Roome and Kuhn⁴⁵ have recently proposed a fast two-photon imaging technique that

simultaneously records voltage and calcium signals from the spiny dendrites of PCs in awake mice and described dendritic spikes triggered by strong PF input.

Numerous recent studies, both experimental^{2,34,36,37,46} and computational,^{28,33} have brought significant evidence supporting a heterogeneous dendritic excitability of PCs. The underlying mechanisms which determine the inhomogeneous excitation across the different dendritic branches are associated with various ion channels such as SK,^{34,36,37} BK,² or A-type K channels.^{18,33}

So far, the classical simplifying approach used in PC computational models was to assume that all ion channel densities are uniform in the spiny dendrite.^{8–10,28,30–33,47–49} There are, however, a few pyramidal cell models, in which dendritic ionic channel densities are defined with respect to the path distance from soma.^{50,51}

In light of recent evidence highlighting heterogeneous dendritic excitability,^{2,34,36,37,46} we propose, to our knowledge, the first heterogeneous ion channel density PC model, in which each dendritic branch is characterized by its own set of ion channel conductance densities. Our work is based on two previous models,^{28,33} and continues on the pioneering PC model of De Schutter and Bower.^{8–10} For a deeper understanding of how PC models were created, how they evolved over the last fifty years and how they were able to predict significant dendritic properties, we direct the reader to a review article.¹¹ For a broader understanding, not limited to the cerebellum, of how computational models contributed to uncovering dendritic functions, we recommend a recent review which highlights the importance of developing intertwined computational and experimental methods.⁵²

Heterogeneous parallel fiber thresholds across the dendritic tree

In agreement with previous work,²⁸ our model predicts that in the absence of a sufficiently strong clustered PF input, dendritic responses have a linear increase with PF synapses for all branches.⁵³ When a specific threshold is met, the dendritic responses exhibit a jump caused by a dendritic calcium spike, followed by a plateau. Using our heterogeneous model, we obtained such a bimodal response throughout the entire dendritic tree. However, the PF thresholds, which represent the minimum number of PF input required to produce a dendritic calcium spike, significantly differ depending on the branch (see Figure 5E). The large difference between the thresholds denotes a strongly inhomogeneous excitability due to specific morphology of the dendritic tree which requires further study. Interestingly, similar PF thresholds apply to multiple branch activation when selecting co-activating branches (Figure 7K) such that they belong to different main divisions (Figure 7M). This indicates that although the branches were defined based on morphology, they can act as independent computational units. However, the same does not hold when co-activating neighboring branches or branches located within the same main division where we observed that the PF threshold is significantly lower than when individually activating one branch.

Conclusions

Our pioneering heterogeneous ion channel density model is the first proposed, to our knowledge, in the cerebellum. In the hippocampus, Siegel et al.⁵⁴ had previously addressed channel density dependency on calcium concentration, revealing how a non-uniform distribution of conductances is linked to both morphology and the pattern of synaptic input, and showcasing an intrinsic form of activity-dependent plasticity.

In our model, each branch is characterized by its own set of ion channel conductance densities. Dendritic branch-specific generation of calcium spikes has been intensively studied in the recent years due to its important role in synaptic plasticity and in facilitating information storage.^{22,25,55,56} Our simulations show how altering the biophysical properties leads to a change in the synaptic gain curve from linear to bimodal linear-step-plateau and vice-versa, suggesting that each branch can multiplex at a cellular level. Modulation of intrinsic excitability at a dendritic branch level was proposed in many recent articles via different ion channels such as SK^{34,36} or A-type potassium channels.^{18,33} The immense impact that the intrinsic excitability plasticity of dendritic branches plays in cerebellar learning has been discussed in detail in the work by Ohtsuki et al.^{35,37} Our study is the first to suggest that P-type Calcium channel can modulate the dendritic responses at single branch level. CaP channels are of utmost importance in the cerebellum, they are widely distributed on PC somata and dendrites^{57,58} and mutations in their alpha_1A protein-pore forming subunit have been linked to various neuropathologies^{59–61} such as ataxia, migraine or epilepsy.

Using our heterogeneous model, by tuning CaP conductance densities for each branch, we obtained a uniform response throughout the cell. Our results show how sufficiently strong activated PF input on each branch produces a dendritic calcium spike. However, these PF thresholds vary considerably between the different branches and therefore suggest a strong inhomogeneous excitability across the tree. We examined how morphological properties can affect the excitability of each branch and we discovered that the length of each branch is strongly correlated with the increase in CaP required for triggering the bimodal response. This explains why the larger, more distal branches, do not require any additional increase in P-type calcium channel conductance density and already exhibited a bimodal response.²⁸

By modulating ionic channels at each branch, we were able to compensate for the different branch morphologies, obtaining a uniform response throughout the PC. When studying dendritic spike propagation, we observed that for most branches, the depolarization remains localized in the branch in which PF were activated. The much larger and distal branches, however, tend to depolarize on the nearby significantly smaller branches. For these cases, we observed that increasing Kv4.3_g blocks the spreading of the dendritic spikes. On the other hand, decreasing Kv4.3_g resulted in more spreading depolarizations for the larger branches such as branch 15 (Figures 3J–3L), while for the smaller sized branches such as branch 3 or branch 10 (Figures S4J–S4L), no spreading depolarizations to neighboring branches were detected. The role of Kv4.3 channel in promoting or suppressing the spread of dendritic calcium spikes was previously discussed³³ for the case of complex spikes.

When co-activating different branches of the PC, we observed that most branches function as individual processing units, having a PF threshold equal or larger than the individually activated branches and the propagation of their dendritic calcium spikes is relatively constrained. This leads us to speculate that PCs may be able to actively control and enhance their capacity of information processing.

Limitations of the study

Our heterogeneous PC model, like many other models,^{28,33,49} assumes a uniform PF distribution, with synapses distributed uniformly across each activated branch. This common simplifying modeling approach will be readdressed in future work due to evidence that more distal branches might possess a significantly higher spine density⁶² with each dendritic spine corresponding to one PF input. The proximal dendrites are thought to have less spines due to competition with climbing fibers, which innervate the proximal dendrite.⁶³

The detailed morphology we used in our work corresponds to a PC of a 21-day-old Wistar rat.⁶⁴ As the rats mature, it is well known that NMDA receptors start being expressed in PCs.^{65,66} In particular, NMDA receptors have been shown to be highly expressed in rats at approximately 8 weeks⁶⁵ after birth, and are thought to play a significant role in PF synaptic plasticity.⁶⁶

Moreover, a recent study⁶⁷ compares PC morphology in rodents versus humans, reporting similar morphologies and electroresponsive patterns between the two, while uncovering higher dendritic complexity in humans and larger currents being required to produce action potentials. Interestingly, their results also show that while most mice exhibit only one dendritic trunk stemming from the soma, humans PCs are more likely to be characterized by 2 or 3 dendritic trunks. This distinctiveness in the number of dendritic trunks in PCs across different species was previously reported by Busch and Hansel,⁶⁸ who showed that multi-branched PCs are more common in both mice and humans in the posterior cerebellar hemisphere which is linked to a cognitive role. This raises many interesting scientific questions of whether multi-branched morphologies enable higher functions.

RESOURCE AVAILABILITY

Lead contact

For further information regarding the model please contact the lead contact, G.C. at gabriela.cirtala@gmail.com.

Materials availability

This study did not generate any unique reagents.

Data and code availability

- This is a computational study. No new experimental data has been generated.
- The codes for the model implementation and simulation experiments are available at: <https://modeldb.science/2016138>.
- Simulated data can be recreated based on the [STAR Methods](#) using the publicly available code published on ModelDB.

ACKNOWLEDGMENTS

This work is supported by the Okinawa Institute of Science and Technology Graduate University. We thank the Scientific Computing & Data Analysis Section (SCDA) of OIST for providing access to the OIST computing cluster.

AUTHOR CONTRIBUTIONS

G.C. and E.D.S. conceived this study. G.C. performed all simulations. G.C. and E.D.S. analyzed the data. G.C. and E.D.S. wrote the manuscript.

DECLARATION OF INTERESTS

The authors declare no competing interests.

STAR★METHODS

Detailed methods are provided in the online version of this paper and include the following:

- KEY RESOURCES TABLE
- EXPERIMENTAL MODEL AND STUDY PARTICIPANT DETAILS
- METHOD DETAILS
 - Purkinje cell model implementation
 - Parameter selection goals
- QUANTIFICATION AND STATISTICAL ANALYSIS

SUPPLEMENTAL INFORMATION

Supplemental information can be found online at <https://doi.org/10.1016/j.isci.2024.110756>.

Received: January 22, 2024

Revised: May 17, 2024

Accepted: August 14, 2024

Published: August 20, 2024

REFERENCES

1. Harvey, R.J., and Napper, R.M. (1991). Quantitative studies on the mammalian cerebellum. *Prog. Neurobiol.* 36, 437–463.
2. Rancz, E.A., and Häusser, M. (2006). Dendritic calcium spikes are tunable triggers of cannabinoid release and short-term synaptic plasticity in cerebellar purkinje neurons. *J. Neurosci.* 26, 5428–5437. <https://doi.org/10.1523/JNEUROSCI.5284-05.2006>.
3. Rancz, E.A., and Häusser, M. (2010). Dendritic spikes mediate negative synaptic gain control in cerebellar Purkinje cells. *Proc. Natl. Acad. Sci. USA* 107, 22284–22289. <https://doi.org/10.1073/pnas.1008605107>.
4. Llinás, R., Nicholson, C., Freeman, J.A., and Hillman, D.E. (1968). Dendritic Spikes and Their Inhibition in Alligator Purkinje Cells. *Science* 160, 1132–1135.
5. Llinás, R., and Sugimori, M. (1980). Electrophysiological properties of *in vitro* Purkinje cell dendrites in mammalian cerebellar slices. *J. Physiol.* 305, 197–213.
6. Pellionisz, A., and Szentágothai, J. (1973). Dynamic single unit simulation of a realistic cerebellar network model. *Brain Res.* 49, 83–99.
7. Pellionisz, A., and Llinás, R. (1977). A computer model of cerebellar Purkinje cells. *Neuroscience* 2, 37–48.
8. De Schutter, E., and Bower, J.M. (1994). Simulated responses of cerebellar Purkinje cells are independent of the dendritic location of granule cell synaptic inputs. *Proc. Natl. Acad. Sci. USA* 91, 4736–4740.
9. De Schutter, E., and Bower, J.M. (1994). An active membrane model of the cerebellar Purkinje cell II. Simulation of synaptic responses. *J. Neurophysiol.* 71, 401–419. <https://doi.org/10.1152/jn.1994.71.1.401>.
10. De Schutter, E., and Bower, J.M. (1994). An active membrane model of the cerebellar Purkinje cell I. Simulation of current clamps in slice. *J. Neurophysiol.* 71, 375–400. <https://doi.org/10.1152/jn.1994.71.1.375>.
11. Bower, J.M. (2015). The 40-year history of modeling active dendrites in cerebellar Purkinje cells: Emergence of the first single cell “community model.”. *Front. Comput. Neurosci.* 9, 129. <https://doi.org/10.3389/fncom.2015.00129>.
12. Angelo, K., London, M., Christensen, S.R., and Häusser, M. (2007). Local and global effects of Ih distribution in dendrites of mammalian neurons. *J. Neurosci.* 27, 8643–8653. <https://doi.org/10.1523/JNEUROSCI.5284-06.2007>.
13. Anwar, H., Hong, S., and De Schutter, E. (2012). Controlling Ca²⁺-activated K⁺ channels with models of Ca²⁺ buffering in purkinje cells. *Cerebellum* 11, 681–693. <https://doi.org/10.1007/s12311-010-0224-3>.
14. Swensen, A.M., and Bean, B.P. (2003). Ionic Mechanisms of Burst Firing in Dissociated Purkinje Neurons. *J. Neurosci.* 23, 9650–9663. <https://doi.org/10.1523/JNEUROSCI.23-29-09650.2003>.
15. Akemann, W., and Knöpfel, T. (2006). Interaction of Kv3 potassium channels and resurgent sodium current influences the rate of spontaneous firing of purkinje neurons. *J. Neurosci.* 26, 4602–4612. <https://doi.org/10.1523/JNEUROSCI.5204-05.2006>.
16. Benton, M.D., Lewis, A.H., Bant, J.S., and Raman, I.M. (2013). Iberiotoxin-sensitive and -insensitive BK currents in Purkinje neuron somata. *J. Neurophysiol.* 109, 2528–2541. <https://doi.org/10.1152/jn.00127.2012>.
17. Sacco, T., and Tempia, F. (2002). A-type potassium currents active at subthreshold potentials in mouse cerebellar Purkinje cells. *J. Physiol.* 543, 505–520. <https://doi.org/10.1113/jphysiol.2002.022525>.
18. Otsu, Y., Marcaggi, P., Feltz, A., Isope, P., Kollo, M., Nusser, Z., Mathieu, B., Kano, M., Tsujita, M., Sakimura, K., and Dieudonné, S. (2014). Activity-dependent gating of calcium spikes by A-type K⁺ channels controls climbing fiber signaling in purkinje cell dendrites. *Neuron* 84, 137–151. <https://doi.org/10.1016/j.neuron.2014.08.035>.
19. Llinás, R., and Sugimori, M. (1980). Electrophysiological properties of *in vitro* Purkinje cell somata in mammalian cerebellar slices. *J. Physiol.* 305, 171–195.
20. Kitamura, K., and Häusser, M. (2011). Dendritic calcium signaling triggered by spontaneous and sensory-evoked climbing fiber input to cerebellar purkinje cells *in vivo*. *J. Neurosci.* 31, 10847–10858. <https://doi.org/10.1523/JNEUROSCI.2525-10.2011>.
21. Schmolesky, M.T., Weber, J.T., De Zeeuw, C.I., and Hansel, C. (2002). The making of a complex spike: Ionic composition and plasticity. *Ann. N. Y. Acad. Sci.* 978, 359–390. <https://doi.org/10.1111/j.1749-6632.2002.tb07581.x>.
22. Losonczy, A., Makara, J.K., and Magee, J.C. (2008). Compartmentalized dendritic plasticity and input feature storage in neurons. *Nature* 452, 436–441. <https://doi.org/10.1038/nature06725>.
23. Makara, J.K., Losonczy, A., Wen, Q., and Magee, J.C. (2009). Experience-dependent compartmentalized dendritic plasticity in rat hippocampal CA1 pyramidal neurons. *Nat. Neurosci.* 12, 1485–1487. <https://doi.org/10.1038/nn.2428>.
24. Branco, T., and Häusser, M. (2010). The single dendritic branch as a fundamental functional unit in the nervous system. *Curr. Opin. Neurobiol.* 20, 494–502. <https://doi.org/10.1016/j.conb.2010.07.009>.
25. Cichon, J., and Gan, W.B. (2015). Branch-specific dendritic Ca²⁺ spikes cause persistent synaptic plasticity. *Nature* 520, 180–185. <https://doi.org/10.1038/nature14251>.
26. Moore, J.J., Robert, V., Rashid, S.K., and Basu, J. (2022). Assessing Local and Branch-specific Activity in Dendrites. *Neuroscience* 489, 143–164. <https://doi.org/10.1016/j.neuroscience.2021.10.022>.
27. Rashid, S.K., Pedrossa, V., Dufour, M.A., Moore, J.J., Chavlis, S., Delatorre, R.G., Poirazi, P., Clopath, C., and Basu, J. (2020). The dendritic spatial code: branch-specific place tuning and its experience-dependent decoupling. Preprint at bioRxiv. <https://doi.org/10.1101/2020.01.24.916643>.
28. Zang, Y., and De Schutter, E. (2021). The cellular electrophysiological properties underlying multiplexed coding in purkinje cells. *J. Neurosci.* 41, 1850–1863. <https://doi.org/10.1523/JNEUROSCI.1719-20.2020>.
29. Hong, S., Negrello, M., Junker, M., Smilgin, A., Thier, P., and De Schutter, E. (2016). Multiplexed coding by cerebellar Purkinje neurons. *Elife* 5, e13810. <https://doi.org/10.7554/elife.13810.001>.
30. Forrest, M.D., Wall, M.J., Press, D.A., and Feng, J. (2012). The Sodium-Potassium Pump Controls the Intrinsic Firing of the Cerebellar Purkinje Neuron. *PLoS One* 7, e51169. <https://doi.org/10.1371/journal.pone.0051169>.
31. Forrest, M.D. (2014). Intracellular calcium dynamics permit a Purkinje neuron model to perform toggle and gain computations upon its inputs. *Front. Comput. Neurosci.* 8, 86. <https://doi.org/10.3389/fncom.2014.00086>.
32. Solinas, S.M.G., Maex, R., and De Schutter, E. (2006). Dendritic amplification of inhibitory postsynaptic potentials in a model Purkinje cell. *Eur. J. Neurosci.* 23, 1207–1218. <https://doi.org/10.1111/j.1460-9568.2005.04564.x>.
33. Zang, Y., Dieudonné, S., and De Schutter, E. (2018). Voltage- and Branch-Specific Climbing Fiber Responses in Purkinje Cells. *Cell Rep.* 24, 1536–1549. <https://doi.org/10.1016/j.celrep.2018.07.011>.
34. Ohtsuki, G., Piochon, C., Adelman, J.P., and Hansel, C. (2012). SK2 channel modulation contributes to compartment-specific dendritic plasticity in cerebellar Purkinje cells. *Neuron* 75, 108–120. <https://doi.org/10.1016/j.neuron.2012.05.025>.
35. Ohtsuki, G., Shishikura, M., and Ozaki, A. (2020). Synergistic excitability plasticity in cerebellar functioning. *FEBS J.* 287, 4557–4593. <https://doi.org/10.1111/febs.15355>.
36. Ohtsuki, G., and Hansel, C. (2018). Synaptic Potential and Plasticity of an SK2 Channel Gate Regulate Spike Burst Activity in Cerebellar Purkinje Cells. *iScience* 1, 49–54. <https://doi.org/10.1016/j.isci.2018.02.001>.
37. Ohtsuki, G. (2020). Modification of synaptic-input clustering by intrinsic excitability plasticity on cerebellar purkinje cell dendrites. *J. Neurosci.* 40, 267–282. <https://doi.org/10.1523/JNEUROSCI.3211-18.2019>.
38. Womack, M., and Khodakhah, K. (2002). Active Contribution of Dendrites to the Tonic and Trimodal Patterns of Activity in Cerebellar Purkinje Neurons. *J. Neurosci.* 22, 10603–10612.
39. Vetter, P., Roth, A., and Häusser, M. (2001). Propagation of Action Potentials in Dendrites Depends on Dendritic Morphology. *J. Neurophysiol.* 85, 926–937.
40. Zhou, H., Lin, Z., Voges, K., Ju, C., Gao, Z., Bosman, L.W.J., Ruigrok, T.J.H., Hoebeek, F.E., De Zeeuw, C.I., and Schonewille, M. (2014). Cerebellar modules operate at different frequencies. *Elife* 3, e02536. <https://doi.org/10.7554/elife.02536>.

41. Wilms, C.D., and Häusser, M. (2015). Reading out a spatiotemporal population code by imaging neighbouring parallel fibre axons *in vivo*. *Nat. Commun.* 6, 6464. <https://doi.org/10.1038/ncomms7464>.
42. Najafi, F., Giovannucci, A., Wang, S.S.H., and Medina, J.F. (2014). Coding of stimulus strength via analog calcium signals in Purkinje cell dendrites of awake mice. *Elife* 3, e03663. <https://doi.org/10.7554/elife.03663>.
43. Najafi, F., Giovannucci, A., Wang, S.S.H., and Medina, J.F. (2014). Sensory-driven enhancement of calcium signals in individual purkinje cell dendrites of awake mice. *Cell Rep.* 6, 792–798. <https://doi.org/10.1016/j.celrep.2014.02.001>.
44. Roome, C.J., and Kuhn, B. (2018). Simultaneous dendritic voltage and calcium imaging and somatic recording from Purkinje neurons in awake mice. *Nat. Commun.* 9, 3388. <https://doi.org/10.1038/s41467-018-05900-3>.
45. Roome, C.J., and Kuhn, B. (2020). Dendritic coincidence detection in Purkinje neurons of awake mice. *Elife* 9, e59619–e59625. <https://doi.org/10.7554/ELIFE.59619>.
46. Ohtsuki, G., Shishikura, M., and Ozaki, A. (2020). Synergistic excitability plasticity in cerebellar functioning. *FEBS J.* 287, 4557–4593.
47. Zang, Y., and De Schutter, E. (2019). Climbing Fibers Provide Graded Error Signals in Cerebellar Learning. *Front. Syst. Neurosci.* 13, 46. <https://doi.org/10.3389/fnsys.2019.00046>.
48. Masoli, S., Solinas, S., and D'Angelo, E. (2015). Action potential processing in a detailed Purkinje cell model reveals a critical role for axonal compartmentalization. *Front. Cell. Neurosci.* 9, 47. <https://doi.org/10.3389/fncel.2015.00047>.
49. Masoli, S., and D'Angelo, E. (2017). Synaptic activation of a detailed Purkinje cell model predicts voltage-dependent control of burst-pause responses in active dendrites. *Front. Cell. Neurosci.* 11, 278. <https://doi.org/10.3389/fncel.2017.00278>.
50. Lazarewicz, M.T., Migliore, M., and Ascoli, G.A. (2002). A new bursting model of CA3 pyramidal cell physiology suggests multiple locations for spike initiation. *Biosystems* 67, 129–137.
51. Kim, H., Jones, K.E., and Heckman, C.J. (2014). Asymmetry in signal propagation between the soma and dendrites plays a key role in determining dendritic excitability in motoneurons. *PLoS One* 9, e95454. <https://doi.org/10.1371/journal.pone.0095454>.
52. Poirazi, P., and Papoutsi, A. (2020). Illuminating dendritic function with computational models. *Nat. Rev. Neurosci.* 21, 303–321. <https://doi.org/10.1038/s41583-020-0301-7>.
53. Walter, J.T., and Khodakham, K. (2006). The linear computational algorithm of cerebellar Purkinje cells. *J. Neurosci.* 26, 12861–12872. <https://doi.org/10.1523/JNEUROSCI.4507-05.2006>.
54. Siegel, M., Marder, E., and Abbott, L.F. (1994). Activity-dependent current distributions in model neurons (activity-dependent regulation/neuronal plasticity/calcium-dependent modulation/channel density). *Proc. Natl. Acad. Sci. USA* 91, 11308–11312.
55. Polksy, A., Mel, B.W., and Schiller, J. (2004). Computational subunits in thin dendrites of pyramidal cells. *Nat. Neurosci.* 7, 621–627. <https://doi.org/10.1038/nn1253>.
56. Govindarajan, A., Israely, I., Huang, S.Y., and Tonegawa, S. (2011). The Dendritic Branch Is the Preferred Integrative Unit for Protein Synthesis-Dependent LTP. *Neuron* 69, 132–146. <https://doi.org/10.1016/j.neuron.2010.12.008>.
57. Llinás, R., Sugimori, M., Hillman, D.E., and Cherksey, B. (1992). Distribution and functional significance of the P-type voltage-dependent Ca²⁺ channels in the mammalian central nervous system. *Trends Neurosci.* 15, 351–355.
58. Usowicz, M.M., Sugimori, M., Cherksey, B., and Llinás, R. (1992). P-type Calcium Channels in the kmata and Dendrites of Adult Cerebellar Purkinje Cells. *Neuron* 9, 1185–1199.
59. Zhuchenko, O., Bailey, J., Bonnen, P., Ashizawa, T., Stockton, D.W., Amos, C., Dobyns, W.B., Subramony, S.H., Zoghbi, H.Y., and Lee, C.C. (1997). Autosomal dominant cerebellar ataxia (SCA6) associated with small polyglutamine expansions in the a 1 A-voltage-depen dent calcium channel. *Nat. Genet.* 15, 62–69.
60. Jun, K., Piedras-Rentería, E.S., Smith, S.M., Wheeler, D.B., Beom Lee, S., Lee, T.G., Chin, H., Adams, M.E., Scheller, R.H., Tsien, R.W., et al. (1999). Ablation of PQ-type Ca²⁺ channel currents, altered synaptic transmission, and progressive ataxia in mice lacking the 1A-subunit. *Proc. Natl. Acad. Sci. USA* 96, 15245–15250.
61. Nimmrich, V., and Gross, G. (2012). P/Q-type calcium channel modulators. *Br. J. Pharmacol.* 167, 741–759. <https://doi.org/10.1111/j.1476-5381.2012.02069.x>.
62. Heintz, T.G., Eva, R., and Fawcett, J.W. (2016). Regional regulation of purkinje cell dendritic spines by integrins and Eph/ephrins. *PLoS One* 11, e0158558. <https://doi.org/10.1371/journal.pone.0158558>.
63. Cesa, R., and Strata, P. (2009). Axonal competition in the synaptic wiring of the cerebellar cortex during development and in the mature cerebellum. *Neuroscience* 162, 624–632. <https://doi.org/10.1016/j.neuroscience.2009.02.061>.
64. Roth, A., and Häusser, M. (2001). Compartmental models of rat cerebellar Purkinje cells based on simultaneous somatic and dendritic patch-clamp recordings. *J. Physiol.* 535, 445–472. <https://doi.org/10.1111/j.1469-7793.2001.00445.x>.
65. Piochon, C., Irinopoulou, T., Brusciano, D., Bailly, Y., Mariani, J., and Levenes, C. (2007). NMDA receptor contribution to the climbing fiber response in the adult mouse Purkinje cell. *J. Neurosci.* 27, 10797–10809. <https://doi.org/10.1523/JNEUROSCI.2422-07.2007>.
66. Piochon, C., Levenes, C., Ohtsuki, G., and Hansel, C. (2010). Purkinje cell NMDA receptors assume a key role in synaptic gain control in the mature cerebellum. *J. Neurosci.* 30, 15330–15335. <https://doi.org/10.1523/JNEUROSCI.4344-10.2010>.
67. Masoli, S., Sanchez-Ponce, D., Vrieler, N., Abu-Haya, K., Lerner, V., Shahar, T., Nedeaescu, H., Rizza, M.F., Benavides-Piccione, R., DeFelipe, J., et al. (2024). Human Purkinje cells outperform mouse Purkinje cells in dendritic complexity and computational capacity. *Commun. Biol.* 7, 5. <https://doi.org/10.1038/s42003-023-05689-y>.
68. Busch, S.E., and Hansel, C. (2023). Climbing fiber multi-innervation of mouse Purkinje dendrites with arborization common to human. *Science* 381, 420–427.

STAR★METHODS

KEY RESOURCES TABLE

REAGENT or RESOURCE	SOURCE	IDENTIFIER
Software and algorithms		
NEURON 8.2	NEURON	https://neuron.yale.edu/neuron/
MATLAB R2022a	Mathworks	https://www.mathworks.com/products/matlab.html
Code generated for publication	ModelDB	https://modeldb.science/2016138

EXPERIMENTAL MODEL AND STUDY PARTICIPANT DETAILS

This is a computational study and therefore, it does not report any experimental model.

METHOD DETAILS

Purkinje cell model implementation

Our model is a modification of a PC model proposed by Zang and De Schutter,²⁸ which consists of four parts: the soma, axon initial segment, smooth dendrites, and spiny dendrites. The initial conductance densities for the four compartments are given in Table S1. All simulations were implemented in NEURON 8.2, while for the analysis and plots we used MATLAB R2022a. The codes are available on ModelDB.

The model encompasses many different ion channels such as voltage-dependent sodium channels, voltage-dependent potassium channels (Kv1, Kv4.3), voltage dependent T-type and P-type calcium channels (CaP), large conductance calcium activated potassium channels (BK), small conductance calcium activated potassium channels (SK2). These channels were added to the model in agreement with recent experimental findings and were discussed in detail in the previous work by Zang et al.^{28,33} In this work, we focus on the voltage dependent P-type calcium channel whose maximum conductance we alter for each dendritic branch of the PC, in order to obtain a bimodal response. In addition to the voltage dependent CaP_g, we have also modified Kv4.3_g for blocking the depolarization of the more distal branches onto the smaller neighboring branches. All conductance densities used in the heterogenous model are shown in Figures 5C and 5D and in Table S2. The PF synapses were approximated using a biexponential waveform²⁸ with rising time $\tau_0 = 0.3\text{ms}$, a decay time $\tau_1 = 3\text{ms}$, a peak conductance $g_{max} = 0.5\text{nS}$, and a reversal potential of 0mV.

As a first step in our analysis, we extended the number of activated PFs distributed for each branch from a maximum of 80 to 200. The activated PFs are distributed uniformly with respect to the length of each branch.²⁸ This extension led us to observe that, in addition to the four branches whose bimodal response was previously observed,²⁸ there are more branches (5, 9, 13 and 15) that exhibit similar response (see Figure 5A).

Parameter selection goals

In developing the first heterogeneous ion channel density model, our main goal was to achieve a bimodal linear-step-plateau response for each activated branch, while constraining the dendritic calcium spikes propagation. Our parameter selection was done such that:

1. Each activated branch shows a bimodal response with a minimum -10mV jump.
2. The dendritic spikes originating in each activated branch remain relatively constrained within the branch and do not propagate towards the neighboring branches ($V > -35\text{mV}$).

For each branch in the dendritic tree, we selected minimum two points: one distal point and one point located in the vicinity of the smooth dendrite. We calculated the dendritic responses with respect to increasing numbers of activated PFs and we determined whether they show bimodal linear-step-plateau or linear response. For the branches which exhibited a linear response, we gradually increased the CaP_g until a bimodal response was obtained. All the other parameters were kept constant as defined in Table S1. We selected the minimum CaP_g value increase required to obtain a bimodal response with a jump of minimum -10mV. For each of these simulations, we analyzed how the dendritic spikes propagate for different number of activated PFs and whether this response remains local or propagates to the nearby branches. In the cases where the propagation onto the nearby branches was very large, we blocked it using increases in Kv4.3 maximum conductance.

The largest PF threshold at which any branch attains its bimodal response is 106PF and corresponds to branch 15. All simulations were run for PF numbers between 10 and 200, with a step of 2PF. As no jumps were detected after 106PF, when plotting the results, we used a maximum of 120PF for simplicity.

QUANTIFICATION AND STATISTICAL ANALYSIS

When analyzing the morphological properties of the branches ([Figures 6B and 6C](#)) we used Matlab curve fitting toolbox to find the best fit for our data: a sum of exponentials $f(x) = a \cdot \exp(bx) + c \cdot \exp(dx)$, with coefficients $a = 1.34e+04$, $b = -3.444$, $c = 130$ and $d = 0.01139$ for panel B and $a = 801.5$, $b = -2.207$, $c = 82.18$ and $d = 0.2742$ for panel C.

Due to the small step of 2PF considered between simulations, and the uniform distribution of PF synapses for each number used, we sometimes observed small noise in the dendritic responses with increasing PF synapses (see for example [Figure S5B](#)). This was not captured before due to the much larger step used.²⁸ However, the small step allowed us to determine more precisely the PF threshold and compare it to the threshold when co-activating two branches. The branch co-activation was done by simultaneously activating the same number of PF synapses on two different branches. Each pair of co-activated branches have same parameters (Kv4.3_g and CaP_g) as in the individually activated scenario (given in [Figure 5](#)). When analyzing the spreading depolarizations in the case of co-activated branches ([Figure 7L](#)), we counted how many additional branches, other than the 2 activated branches, show depolarizations larger than a set threshold of -35mV. Due to the noise described above, we imposed the additional condition that this condition must be met for activation of minimum 7 different numbers of PF.